Time-Distance Helioseismology. II

Alexander Kosovichev
Stanford University

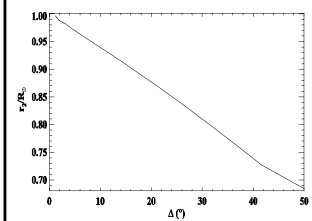

The lower turning point r_2 is plotted as a function of the travel distance for acoustic rays with temporal frequency $\omega/2\pi = 3.1\text{mHz}$.

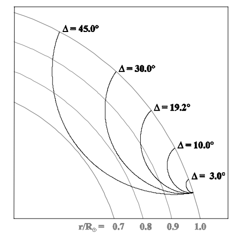

A great circle plane containing several sample rays. The grey arcs indicate the fractional radius, and the five black curves show the path taken by waves propagating in the convection zone. The largest ray shown travels a distance of 45° and reaches to $r = 0.71R$

Problem: Show that for the convection zone the depth of the lower turning point is approximately $R\Delta/\pi$.

Sound-speed profile (JC-D's Model S)

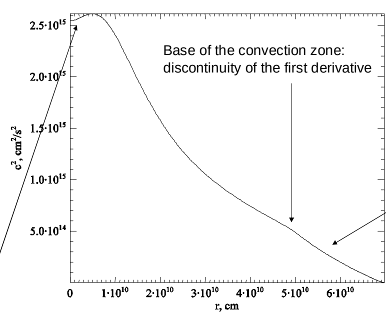

Why is the sound speed lower in the core?

Wave reflection from the bottom of the convection zone

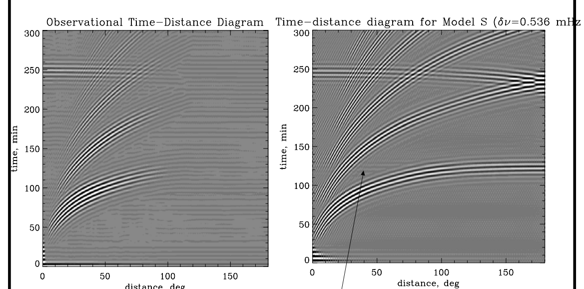

Very weak reflection signal in the theoretical diagram

Cross-covariance function for surface gravity waves (f-mode)

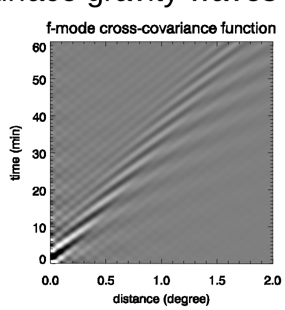

Dispersion relation for f-mode is $\omega^2 = gk$

The group speed is a half of the phase speed.

Why does the cross-covariance function for f-modes look different from the p-mode one?

Plan

- Time-distance diagnostics
  - Fermat's principle
  - Effects of magnetic field
  - Finite wavelength effects
    - Born approximation
    - Phase-speed filtering
- Time-distance results
  - Synoptic maps of subphotospheric flows
  - Meridional circulation
  - Structure and dynamics of sunspots
  - Emerging active regions
  - Shear flows in flaring active regions
- Time-distance perspectives
  - Solar-B and SDO space missions
  - Helioseismology after Solar-B and SDO

Some comments on terminology

- The term *"helioseismology"* was suggested by Douglas Gough about 30 years ago and first appeared in 1979 in a paper by Severny et al. It consists of all Greek words and replaced American "solar seismology".
- For other stars the correct term is "asteroseismology" (not astroseismology) because "astero" is a Greek word and "astr" is Latin. The first helioseismology rule is not mix languages in one word. (D.O. Gough, 1996, The Observatory, v. 116, p. 313-315)
- Recently, a new term "magnetohelioseismology" was invented. However, this is not acceptable because "magnet" is Latin. The original Greek word is "magnes" (from Magnesia).
- What about "Time-distance helioseismology"?

If you want to express this in a single word then the correct term is "telechronohelioseismology".

However, we keep "time-distance helioseismology" because TD also means Tom Duvall who invented this field.

A bit of history

- NASA Solar Physics Exploration Seminar (April 10, 1991).
  - Speaker: Douglas Gough

Gough's Law

- All initial results of helioseismology are incorrect.

Time-distance diagnostics

Fermat's Principle

A powerful property of ray paths is that they obey Fermat's Principle, which states that the travel time along the ray is stationary with respect to small changes in the path. This implies that if a small perturbation is made to the background state, the ray path is unchanged.

The perturbation to the travel time can then be expressed as

$$\tau - \tau_0 = \frac{1}{\omega}\int_{\Gamma_0} \delta k \, ds.$$

Here δk is the perturbation to the wavevector due to inhomogeneities in the background state, and Fermat's principle allows us to make the integral along the unperturbed ray path Γ_0.

In the solar convection zone, the Brunt-Väisälä frequency N is small compared to the acoustic cutoff frequency and the typical frequencies of solar oscillations. Neglecting this frequency, the dispersion relation can be written as

$$k_r^2 = \frac{1}{c^2}\left(\omega^2 - \omega_C^2\right) - k_h^2,$$

$$k_h^2 = \frac{l(l+1)}{r^2}.$$

If we allow small perturbations (relative to the background state) in ω, c^2, and ω_C^2, then the integrand in Fermat's equation can be written to first order as

$$\frac{\delta k \, ds}{\omega} = \left[\frac{\delta\omega}{c^2 k} - \left(\frac{\delta c}{c}\right)\frac{k}{\omega} - \left(\frac{\delta\omega_C}{\omega_C}\right)\left(\frac{\omega_C^2}{c^2\omega^2}\right)\frac{\omega}{k}\right] ds,$$

where I have neglected terms which are second-order in $\delta c/c$ and $|u|/c$.

Effect of velocity field

One possible perturbation to the spherically symmetric background state is a velocity field. If the flow field is described by $\mathbf{u}$ then the observed frequency will be Doppler shifted by the advection of the oscillations,

$$\delta\omega = -k\hat{\mathbf{n}}\cdot\mathbf{u},$$

so that the Fermat's equation becomes

$$\tau^{\pm} - \tau_0 = -\int_{\Gamma_0}\left[\frac{\mathbf{u}\cdot(\pm\hat{\mathbf{n}})}{c^2} + \left(\frac{\delta c}{c}\right)\frac{k}{\omega} + \left(\frac{\delta\omega_C}{\omega_C}\right)\left(\frac{\omega_C^2}{c^2\omega^2}\right)\frac{\omega}{k}\right]ds,$$

where $\hat{\mathbf{n}}$ is a unit vector tangent to the ray path. Here I have defined the quantity τ^{+} as the perturbed travel time in one direction along the ray path (unit vector $+\hat{\mathbf{n}}$) and τ^{-} as the perturbed travel time in the opposite (reciprocal) direction (unit vector $-\hat{\mathbf{n}}$).

Separation of the velocity field signal from the other perturbations

To separate the effects of the velocity field from the other perturbations, we thus define

$$\delta\tau_{\rm diff} \equiv \tau^{+} - \tau^{-} = -2\int_{\Gamma_0}\frac{\mathbf{u}\cdot\hat{\mathbf{n}}}{c^2}ds$$

$$\delta\tau_{\rm mean} \equiv \frac{(\tau^{+}+\tau^{-})}{2} = \tau_0 - \int_{\Gamma_0}\left[\left(\frac{\delta c}{c}\right)\frac{k}{\omega} + \left(\frac{\delta\omega_C}{\omega_C}\right)\left(\frac{\omega_C^2}{c^2\omega^2}\right)\frac{\omega}{k}\right]ds.$$

This equation thus provides the link between the measured travel time differences and the flow field along the ray path. This simple equation is in the heart of the time-distance helioseismology.

Magnetic field effects

- Magnetic field in sunspots, particularly, in the sunspot umbra may significantly affect the time-distance diagnostics for 3 main reasons:
  - The standard Doppler shift measurements may not provide accurate estimate of the actual line-of-sight velocity
  - Magnetic field inhibits convection (reducing excitation) and presumably absorbs waves causing inhomogeneous distribution of the acoustic power on the solar surface, resulting systematic shifts in the standard travel times (Woodard's effect)
  - Magnetic field causes changes in the dispersion properties of acoustic waves resulting in anisotropy in the travel times
- Magnetic effects are particularly strong when plasma parameter is of the order of unity or smaller: $\beta = 4\pi P/B^2 \leq 1$
- For most sunspot models this happens above the photosphere. This regime is poorly understood, and avoid this we mostly work with low-frequency waves that are reflected below the photosphere.
- At high frequencies, magnetic effects ("shower-glass effect", "inclined field effect") become strong, particularly, in acoustic holography (Doug Braun's talk tomorrow). Our tests show that for time-distance measurements these are much less significant.

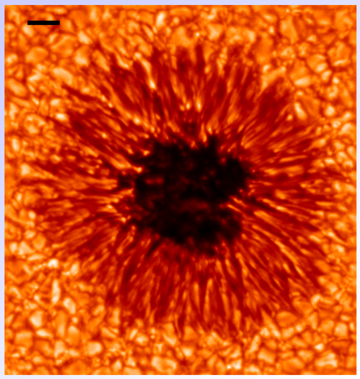

MHS field configuration

B(axis)=2000 G

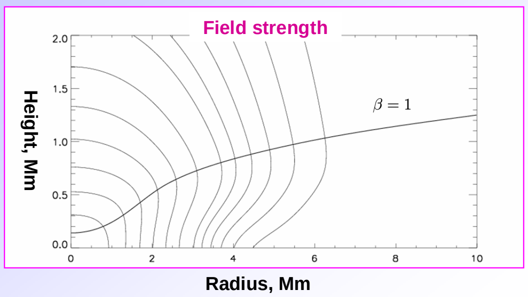

MHS field configuration

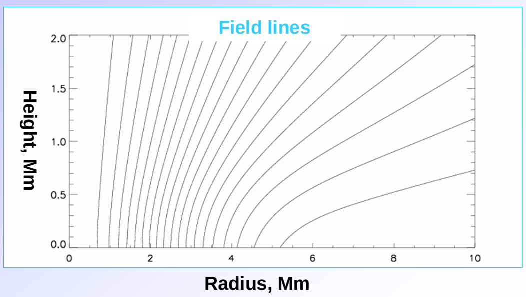

Numerical simulations of the interaction of acoustic waves with magnetic field of sunspots (E.Khomenko, 2005)

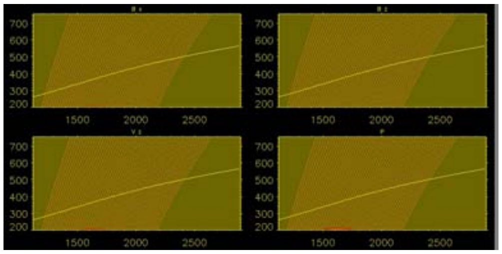

Ray theory for magnetic field (plasma parameter β > 1)

Wave dispersion relation $(\omega - \vec{k}\cdot\vec{U})^2 = \omega_c^2 + k^2 c_f^2,$

Fast magneto-acoustic speed
$$c_f^2 = \tfrac{1}{2}\left(c^2 + c_A^2 + \sqrt{\left(c^2 + c_A^2\right)^2 - 4c^2(\vec{k}\cdot\vec{c}_A)^2/k^2}\right)$$

Alfven velocity
$$\vec{c}_A = \vec{B}/\sqrt{4\pi\rho}$$

$$\delta\tau = -\int_\Gamma \left[\frac{(\vec{n}\cdot\vec{U})}{c^2} + \frac{\delta c}{c}S + \left(\frac{\delta\omega_c}{\omega_c}\right)\frac{\omega_c^2}{\omega^2 c^2 S} + \frac{1}{2}\left(\frac{c_A^2}{c^2} - \frac{(\vec{k}\cdot\vec{c}_A)^2}{k^2 c^2}\right)S\right]ds,$$

$$\delta\tau_{\text{mean}} = -\int_\Gamma \left[\frac{\delta c}{c}S + \left(\frac{\delta\omega_c}{\omega_c}\right)\frac{\omega_c^2}{\omega^2 c^2 S} + \frac{1}{2}\left(\frac{c_A^2}{c^2} - \frac{(\vec{k}\cdot\vec{c}_A)^2}{k^2 c^2}\right)S\right]ds.$$

$$\delta\tau_{\text{diff}} = -2\int_\Gamma \frac{(\vec{n}\cdot\vec{U})}{c^2}ds;$$

$S = k/\omega$ is the wave "slowness"

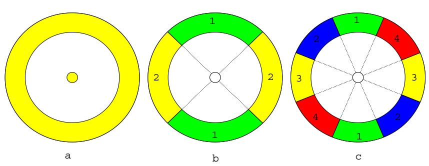

Basic time-distance observing schemes: a) measurements of the mean travel time between a central point and surrounding annuli used for diagnostics of wave-speed perturbations (a combined temperature and magnetic field signal); b) the travel-differences measured in the North-South and East-West directions to deduce the flow velocity; c) a proposed scheme for measuring the travel time anisotropy for diagnostics of sub-surface magnetic field

An initial attempt to measure subphotospheric magnetic field (Junwei Zhao, see also Ryutova & Scherrer 1998, ApJ, v.494, p.438)

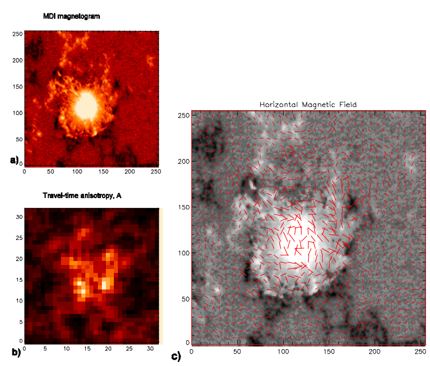

New method for measuring travel times

Example: uniform flow

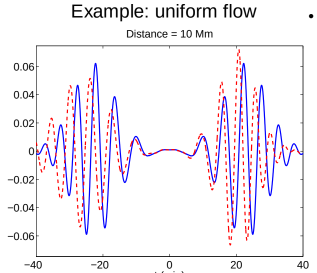

Blue: no flow
Red: 1 km/s

Courtesy: Aaron Birch

- Two methods for measuring travel times:
  - Fit the wavelet (wave-packet model) – Gabor wavelet
  - Calculate the displacement relative to a reference cross-covariance function by cross-correlation (Gizon & Birch, 2002).

This gives a linear relation between the perturbations in the travel time and cross-covariance function.

The perturbation to the cross-covariance function can be calculated for sound-speed perturbations and flows using the Born approximation.

Illustration of the Born-approximation theory

$Lf + \omega^2 f = F_\omega(\vec{r}_s)$ - wave equation with random sources

solution: $f(\vec{r},\vec{r}_s,t) = \int_0^\infty G_\omega(\vec{r},\vec{r}_s)F_\omega(\vec{r}_s)e^{-i\omega t}d\omega.$ $\quad L_0 G_0 + \omega^2 G_0 = \delta(\vec{r}-\vec{r}_s),$

Green's function

$(L_0 + L_1)(G_0 + G_1) + \omega^2(G_0 + G_1) = \delta(\vec{r}-\vec{r}_s).$ $\quad L_0 G_1 + \omega^2 G_1 = L_1(G_0 + G_1).$

$$\boxed{\delta\tau(\Delta) = \int_V K_T(\vec{r},\Delta)\frac{\delta w}{w}d\vec{r}}$$

τ – time; Δ – distance; w – solar property
K – sensitivity kernel

$$K(\Delta,r) = -4\frac{\int d\omega\,\omega\Im\{\Psi_0(\omega)\}\Re\{A_1 + A_2 + A_3\}}{\int d\omega\,\omega^2\Psi_0(\omega)\Psi_0^*(\omega)}$$

- double summation over the global modes

$$A_1 = \sum_{nl} k_{nn}^l(\Delta,r)\,|U^{nl}(R)|^2|S_{nl}(r_s)|^2, \quad A_2 = \sum_{nn'l} k_{nn'}^l(\Delta,r)\,|U^{nl}(R)|^2\, S_{nl}(r_s)S_{n'l},$$

$$A_3 = \sum_{nn'l} k_{nn'}^l(\Delta,r)U^{nl}(R)U^{n'l}(R)\,|S_{nl}(r_s)|^2,$$

U and D –mode eigenfunctions

$$k_{nn'}^l(\Delta,r) = -r^2\rho c^2 D(\omega)b^l F_l^2(\omega)\,|L_{nl}(\omega)|^2\, N_{n'l}(\omega)\frac{2l+1}{4\pi}P_l(\cos\Delta)D^{nl}(r)D^{n'l}(r).$$

Notice mode coupling

Sensitivity kernels for travel-time measurements in the Born approximation

- Properties of the solar interior are related to the measured travel times through sensitivity kernels (e.g. for sound speed):

$$\delta\tau(\Delta) = \int_V K_T(\vec{r},\Delta)\frac{\delta c}{c}dV$$

where integration is over the whole volume of the Sun.

- These kernel are calculated in the Born approximation as in terms as a combination of normal mode eigenfunctions.
- The sound-speed variations, flow velocity and other solar properties are determined from this equation by inversion.

"Banana-doughnut kernel"

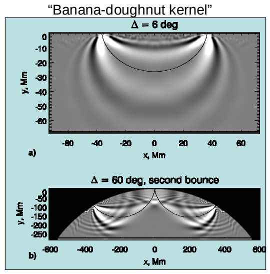

Examples of travel-time sensitivity kernels for the first and second bounces calculated in the Born approximation. The black curves show the corresponding ray paths.

Testing the ray and Born approximations for a simple spherical sound-speed perturbation

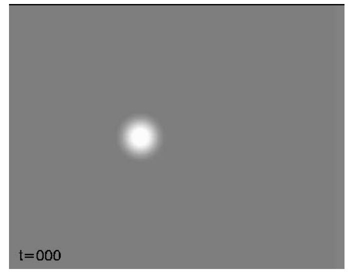

Banana-doughnut structure of the travel-time sensitivity kernels is caused by the wave-healing effect

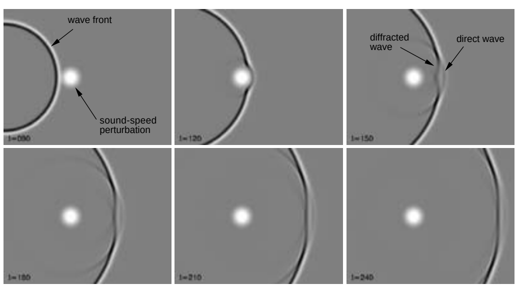

Comparison of the ray and Born approximations with numerical simulations

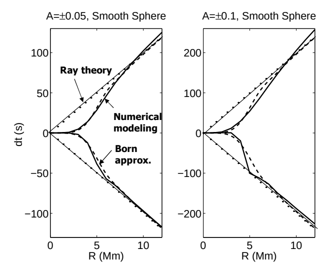

Ray approximation overestimates travel times for small structures. This means that such structures are underestimated in the inversion results.

Born approximation is sufficiently adequate when diffraction effects are not significant.

Phase-speed filtering

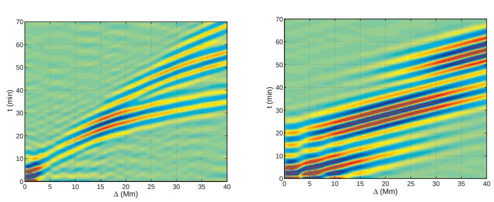

- The filter is tuned to select waves with horizontal phase speed v=ω/k near the ray theory value corresponding to a particular distance Δ.

Courtesy of Aaron Birch

Example of the phase-speed filtering

Filtered power spectrum

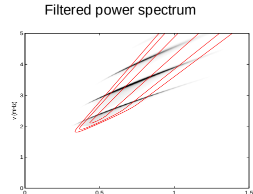

Cross-covariance function

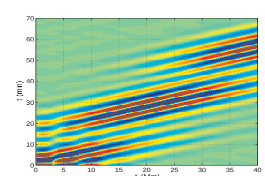

Sound-speed sensitivity kernel

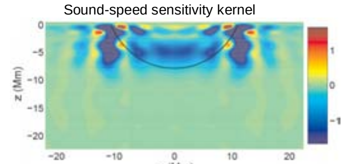

Velocity Kernels (w/ phase-sped filter)

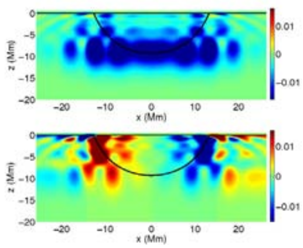

- Sensitivity to horizontal and vertical flows
- Not so different than the ray-theory picture !

Deep- and surface-focusing observing schemes

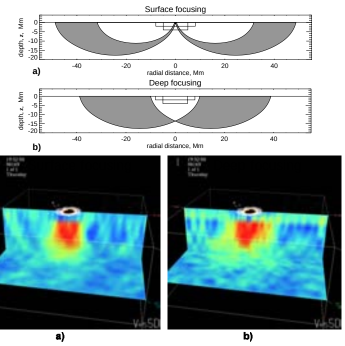

Sound-speed structure beneath a sunspot (Couvidat et al 2005)

Ray approximation (old)

Born theory (new)

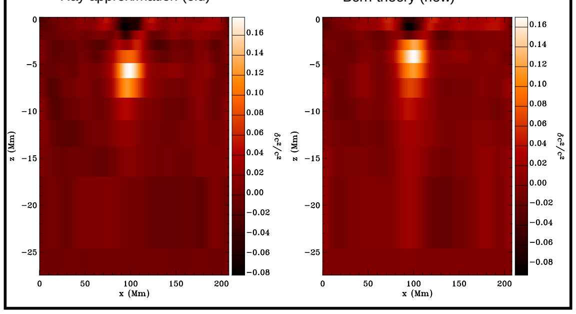

Time-distance results

– Synoptic maps of subphotospheric flows
– Meridional circulation
– Structure and dynamics of sunspots
– Emerging active regions
– Shear flows in flaring active regions

Detailed maps of subsurface flows

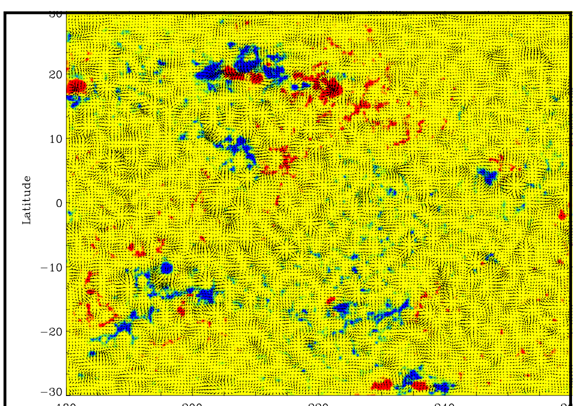

A small sample of a synoptic map of subsurface flows

Solar Subsurface Weather

Synoptic maps of subsurface flows (0-20 Mm)

Depth 2 Mm

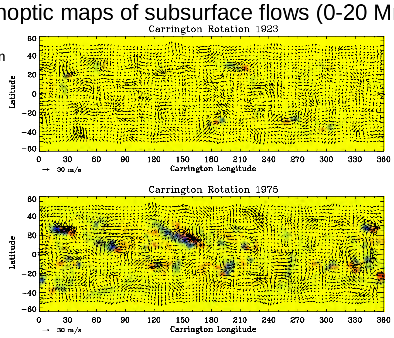

Similar maps are obtained from the ring analysis (Haber et al 2002)

Synoptic maps of subsurface flows (0-20 Mm)

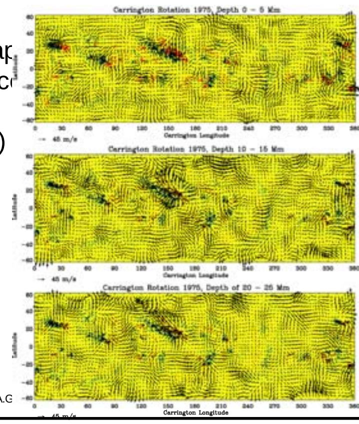

Zhao, J. & Kosovichev, A.G

Large-scale flows around active regions:

(example AR9433, April 2001)

- converging 40 m/s flow toward the neutral line in the upper layers
- diverging flow below 9 Mm

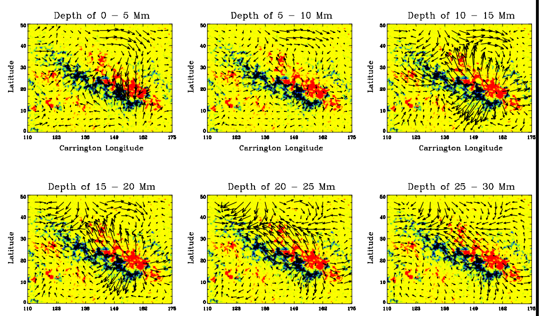

Global characteristics of the synoptic flows for CR 1923

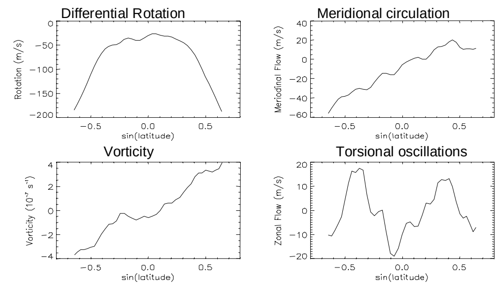

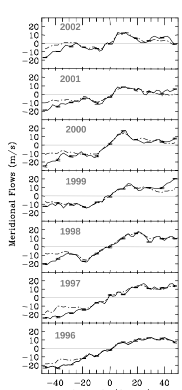

Solar-cycle variations of meridional circulation

- In addition to the mean meridional flow from the equator to the poles we find extra meridional circulation cells converging towards the activity belts and migrating towards the equator as the solar cycle progresses
- Slowing meridional circulation at the solar maximum creates difficulties for flux transport dynamo models to explain reversals of the polar magnetic fields.

Diagnostics of sunspots and emerging active regions

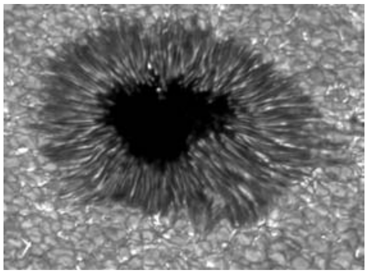

Sunspot structure and dynamics

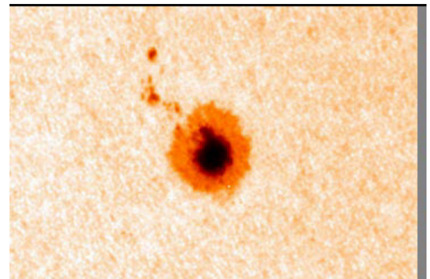

Numerical simulations (N.Hurlburt)

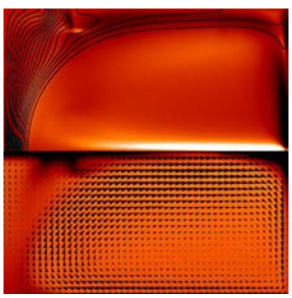

Numerical model of sunspot vs observations

Model
Hurlburt and Rucklidge(2000)

Observations

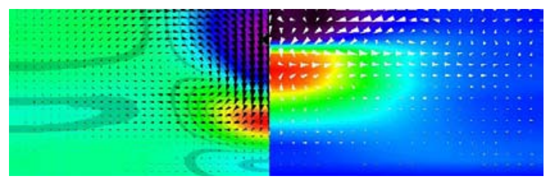

Flow patterns under the sunspot

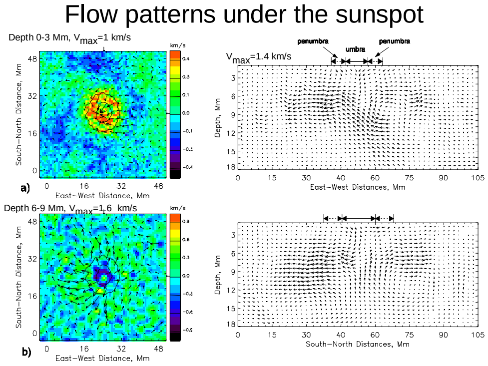

Parker's model

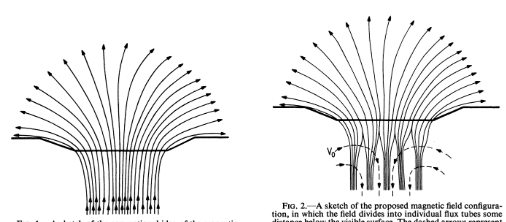

FIG. 1.—A sketch of the conventional idea of the magnetic field configuration of a sunspot. The heavy line represents the visible surface of the Sun.

FIG. 2.—A sketch of the proposed magnetic field configuration, in which the field divides into individual flux tubes some distance below the visible surface. The dashed arrows represent the presumed convective downdraft which helps to hold the separate flux tubes together in the tight cluster that constitutes the sunspot.

Monolithic model

Cluster Model

Helioseismology provides strong evidence for the cluster model.

Observations of emerging active region by time-distance helioseismology

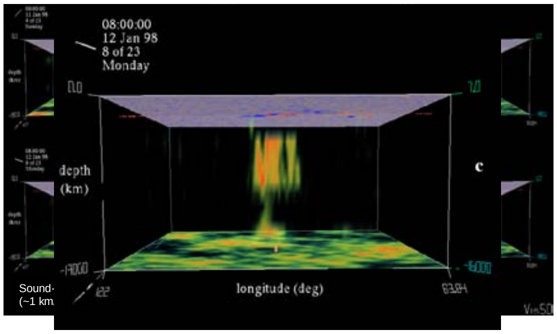

Observation of emerging active region with 2-hr resolution

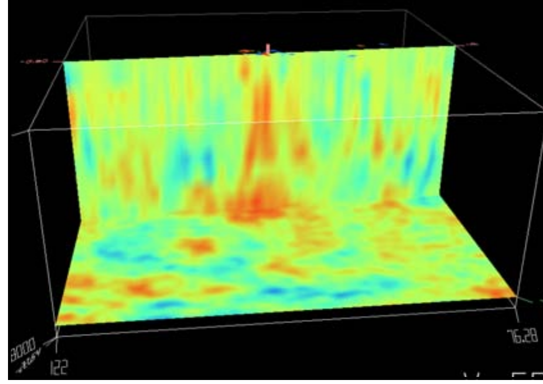

Subphotospheric imaging of active regions

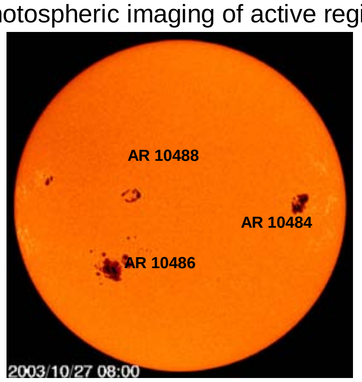

Evolution of AR 10486-488: October 24 – November 2, 2003

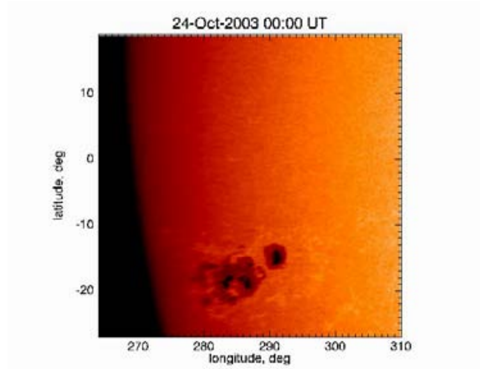

Sound-speed map and magnetogram of AR 10486 on October 25, 2003, 4:00 UT (depth of the lower panel: 45 Mm)

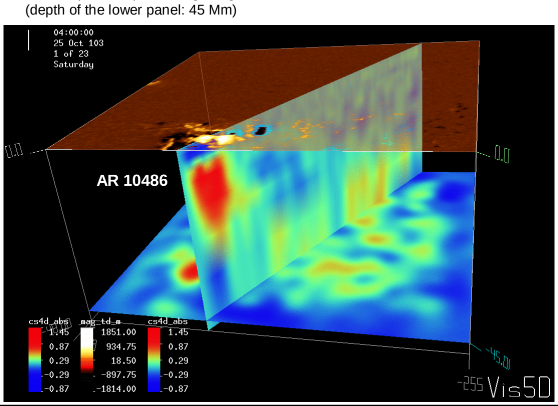

Sound-speed map and magnetogram of AR 10486 on October 26, 2003, 12:00 UT
AR 10488 is emerging

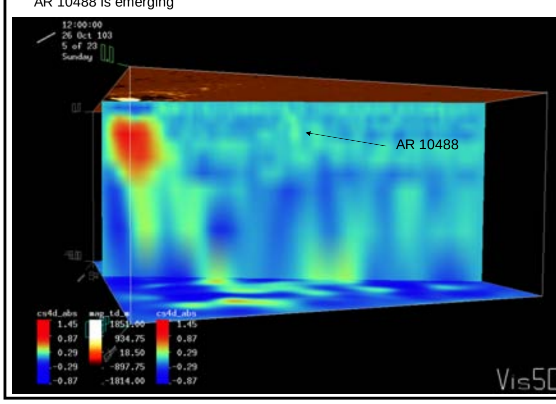

Emergence of AR 10488, October 26, 2003, 20:00 UT

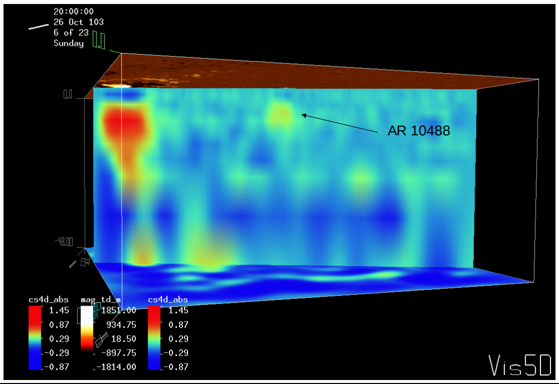

Emergence of AR 10488, October 27, 2003, 4:00 UT

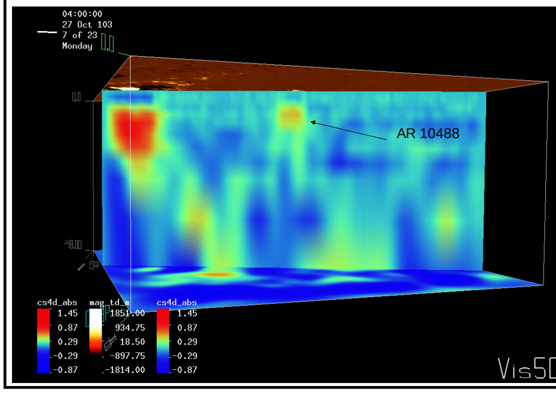

Growth and formation of sunspots of AR 10488, October 29, 2003, 4:00 UT

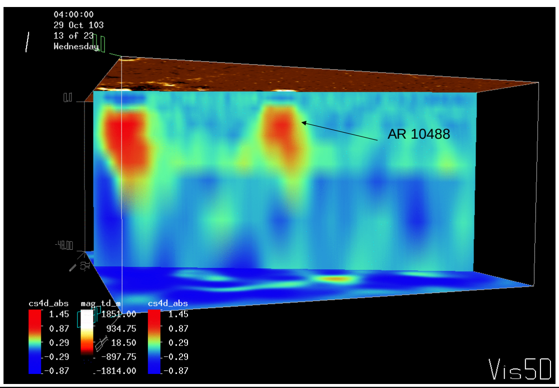

Growth and formation of sunspots of AR 10488, October 31, 2003, 12:00 UT

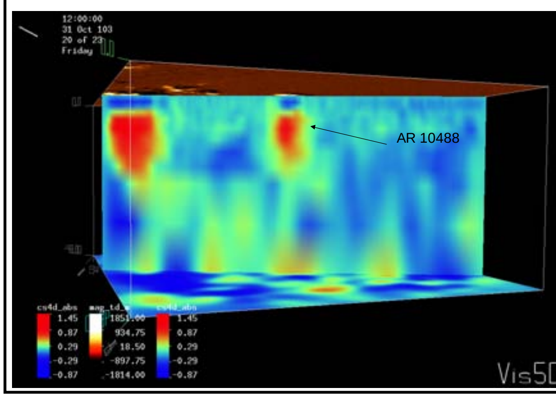

Cut in East-West direction through both magnetic polarities, showing a loop-like structure beneath AR 10488, October 30, 2003, 20:00 UT

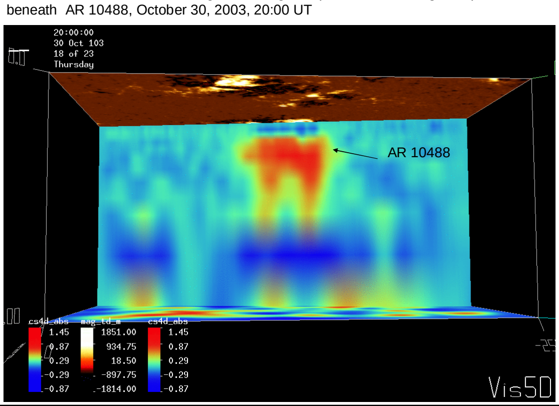

Volume rendering of the sound-speed structures, October 29, 2003, 4:00 UT

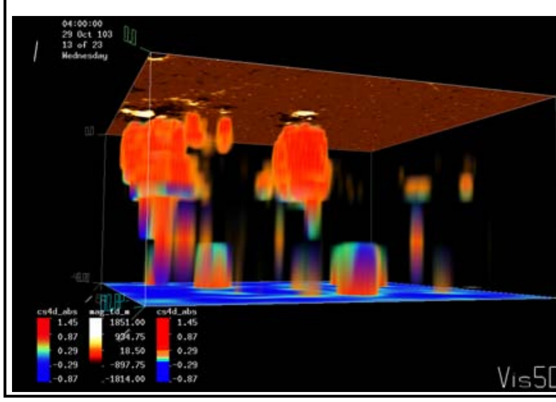

Conclusions for sunspots and active regions

- Helioseismology provides powerful diagnostics of subphotospheric dynamics of active regions and sunspots.
- Sunspots as cool structures appear to be shallow, only about 4-5 Mm deep. The deeper interior is hotter than surrounding plasma.
- Subsurface dynamics of sunspots is dominated by strong converging flows.
- There is evidence for the cluster model of sunspots.
- Magnetic flux tubes in the upper convective zone emerge very rapidly, with a speed greater than 1 km/s.

Magnetic energy release and the internal dynamics

Sunspot dynamics associated with flares and CME

- Magnetic field topology and magnetic stresses in the solar atmosphere are likely be controlled by motions of magnetic flux footpoints below the surface However, the depth of these motions is unknown.
- Time-distance helioseismology provides maps of subphotospheric flows and sound-speed structures, which can be compared with photospheric magnetic fields and X-ray data.

Theoretical example
Magnetic reconnection by flipping (Priest & Demoulin, 1995)

In sheared X-type fields, a smooth continuous shear flow imposed on the boundary across a quasi-separatrix produces a flipping of magnetic field lines as they slip rapidly through plasma in the other quasi-separatrix layer. It results in a strong plasma jetting localized in, and parallel to, the separatrix layers.

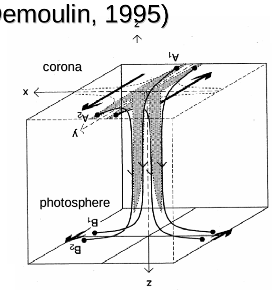

Reconnection by magnetic flipping, driven by a slow continuous foot point motion from B_1 to B_2 and producing a rapid slippage of field lines from A_1 to A_2 in diffusive layers (shaded) near a quasi-separatrix layer.

Fast subphotospheric plasma streams 4-6 Mm below the surface in magnetic field quasi-separatrix areas

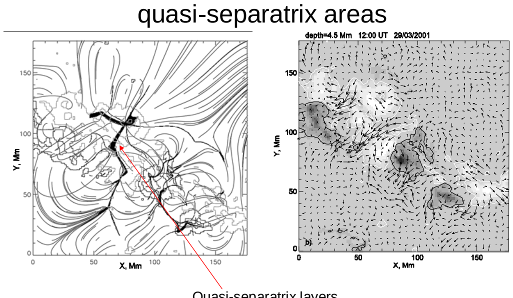

Kulinova et al 2003

Time-distance analysis of 2 flares:

1. X17.2 October 28, 2003, 9:51-11:24 UT
2. X10.0 October 29, 2003, 20:37-21:01 UT

X10 flare, Oct. 29, 2003, 20:37 UT

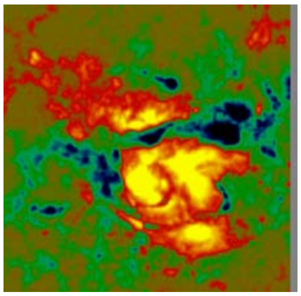

20:28 UT

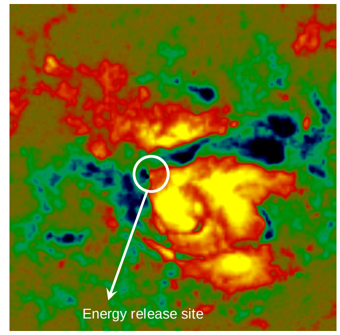

Variations of the longitudinal component of magnetic energy

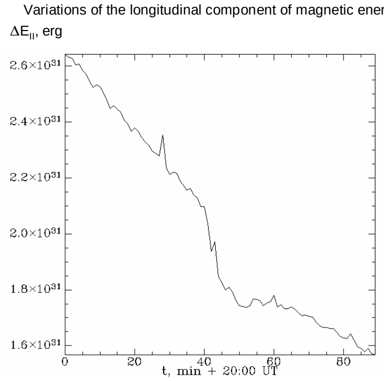

Sub-photospheric flow maps and photospheric magnetograms during X10 flare

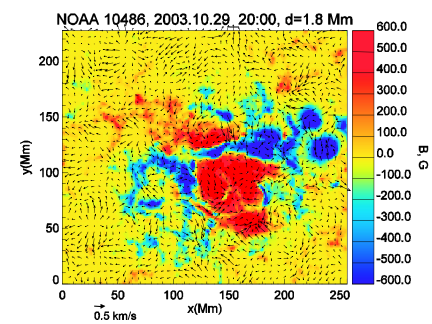

Sub-photospheric flow maps and photospheric magnetograms during X10 flare

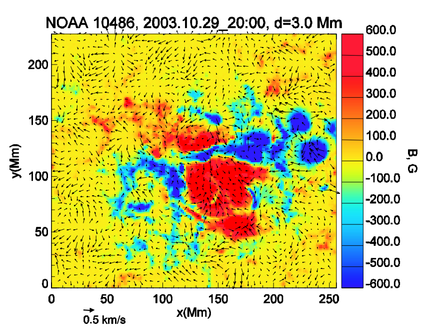

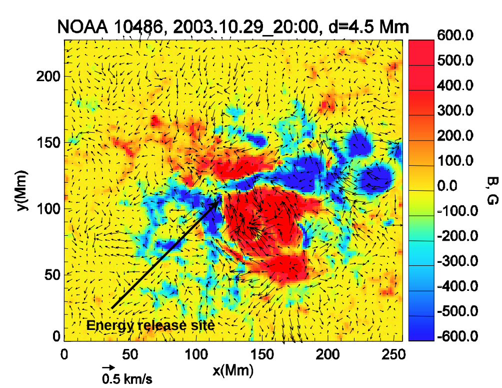

X17.2 flare, Oct. 28, 2003, 9:51 UT

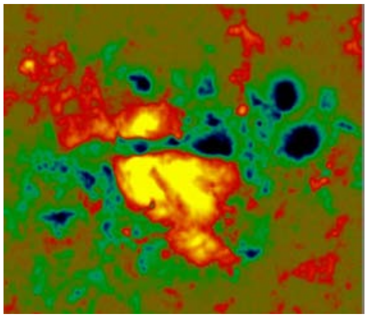

X17.2 flare, Oct. 28, 2003, 9:51 UT

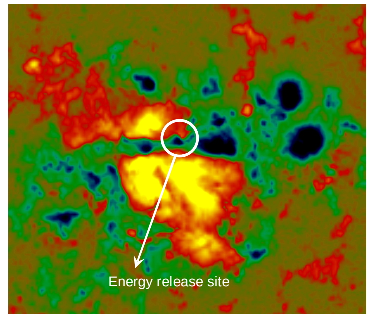

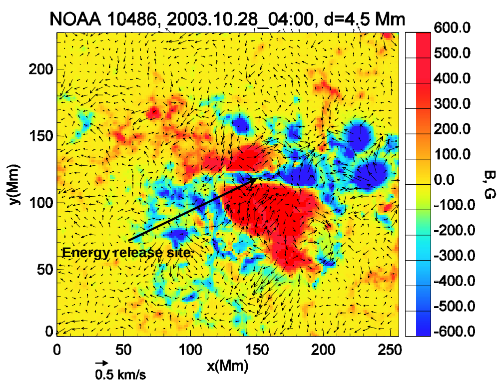

Conclusions for flaring regions

- It appears that the energy-release sites are associated with strong shearing and converging flows at depth 4-6 Mm.
- Further analysis should include more accurate flow maps with higher temporal and spatial resolution, and also magnetic field reconstruction in the corona.

Time-distance perspectives

– Solar-B and SDO space missions
– Helioseismology after Solar-B and SDO

SDO - Solar Dynamics Observatory (launch in 2008)

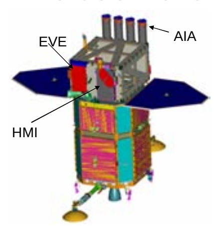

SDO includes:

•**AIA** - The Atmospheric Imaging Array
Lockheed Martin Solar and Astrophysics Lab

•**HMI** – Helioseismic and Magnetic Imager
Stanford University with LMSAL

•**EVE** – EUV Variability Experiment
University of Colorado/LASP

SDO will be in an inclined geosynchronous orbit with data collected at White Sands NM and operations managed at GSFC.

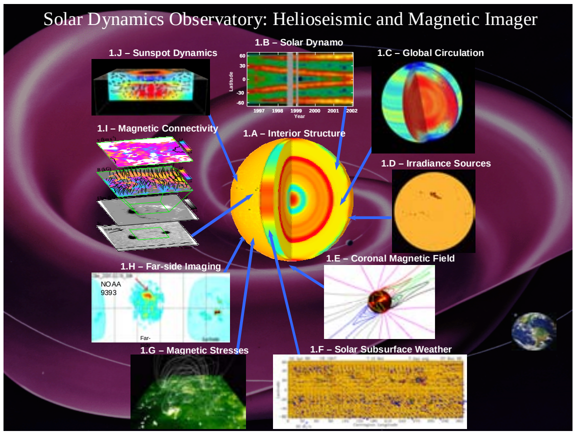

HMI Science Analysis Plan

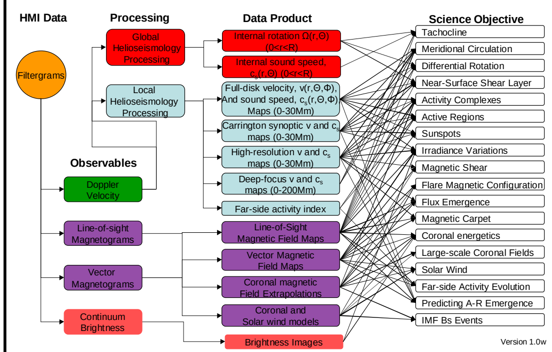

SOLAR-B

Science
- **Coronal heating**
- **Coronal structure / dynamics**
- **Elementary processes in Magnetic Reconnection**

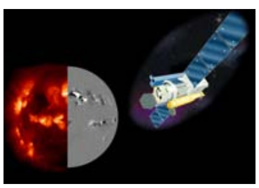

Launch Date:
Summer 2006, with ISAS M-V-7
Orbit:
Sun synchronous altitude ~ 600 km
Weight: ~ 900 kg

Mission instruments
- **Optical Telescope / Vector Magnetograph (SOT)**
- **X-ray Telescope (XRT)**
- **EUV Imaging Spectrometer (EIS)**

High resolution helioseismology

- MDI high-resolution power spectrum
  - No resonant p modes above $l \approx 2000$
  - The f-mode frequency ~ sqrt(l)

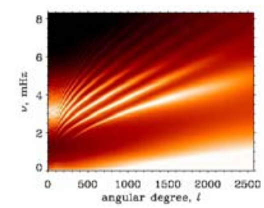

High resolution cross-covariance functions

- Sekii et al 2001: MDI(*left*) versus La Palma SVST (*right*, Berger et al 1998)

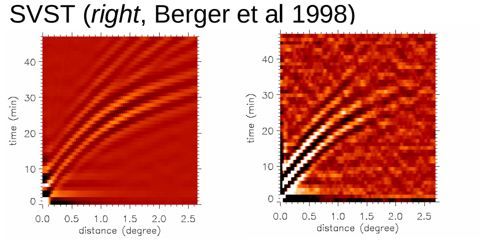

High resolution helioseismology with Solar-B

- La Palma result shows the improvement in (mainly p-mode) time-distance S/N in <10,000 km range, down to <1,000km
- Local helioseismology with high-degree f modes an obvious thing to do, but p-mode seismology will also benefits from SOT high-resolution

Helioseismology after SDO and Solar-B

- Main objectives
  - Investigation of the polar regions (Solar Orbiter, Solar Polar Imager)
  - 3D mapping of the whole interior (Safari)

Stereohelioseismology: time-distance helioseismology of the deep interior (SAFARI mission)

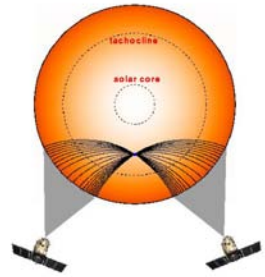

Vision Mission Study

Solar Polar Imager: Observing Solar Activity from a New Perspective

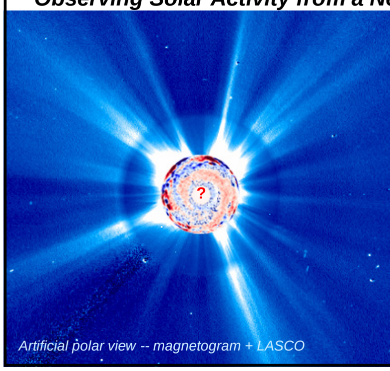

Mission

Spacecraft in highly inclined ~75° heliocentric orbit 0.5AU

Uses solar sail to reach high inclination

Science

Helioseismology & magnetic fields of polar regions

Polar view of corona,CMEs, solar irradiance

Link high latitude solar wind & energetic particles to coronal sources

What is the shape of the tachocline, prolate?

Polar jet?

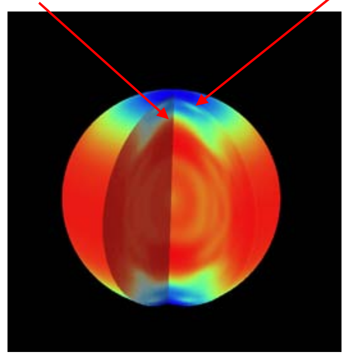

What is the high-latitude structure of the meridional circulation?

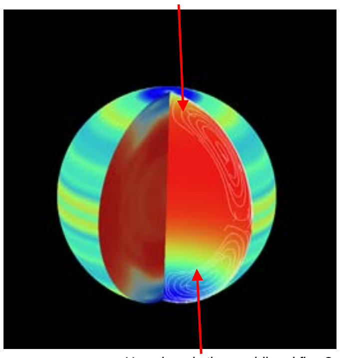

How deep is the meridional flow?

What is the large-scale circulation pattern in polar regions and its role the magnetic field dynamics?

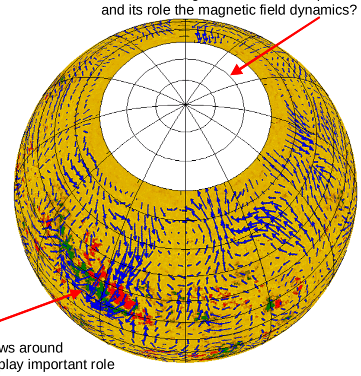

Converging flows around active regions play important role in their evolution.

Some key questions

- Are there multiple meridional cells predicted by numerical simulations?
- How fast is the polar rotation?
- How does the polar rotation changes with the solar cycle?
- Are there fast variations of the polar rotation?
- How deep are these variations?
- Is there a link to rotation of the radiative interior?
- How are these linked to the angular momentum loss?
- …

Solar Sail Propulsion

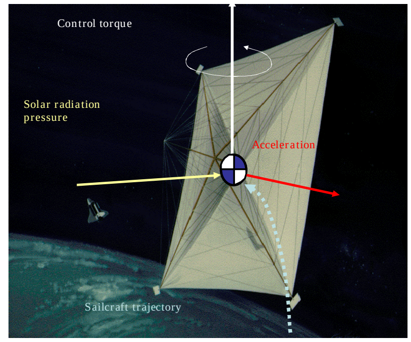

Solar Sail Baseline

Sailcraft
- $10{,}000 m^2$ area
- $14.1 gm/m^2$ areal l
- $0.58 mm/s^2$ accele
- 50 kg payload
- 2µm Mylar sail
- Inflatable deployr
- Sub Tg rigidizatic
- Vane 3-axis ACS
- Scalable structure
- **140.7 kg flight m**

Space Segment
(Sailcraft + Jettisoned E
- 232.9 kg launch n
- $1.7 m^3$ stowed vol
- 92.2 kg jettisoned

Sail Subsystem
- 4.8 gm/m2
- $1.7 mm/s^2$ acceler

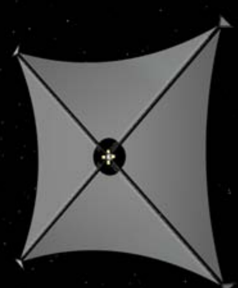

10-m Quadrant System

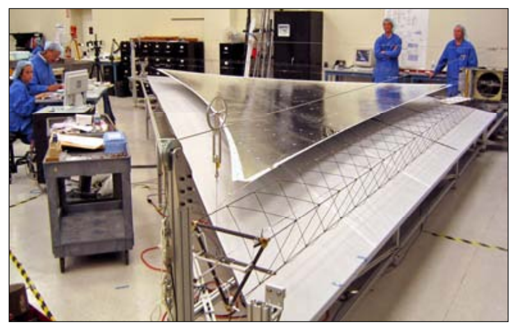

SPI orbit

SPI view of the solar magnetic fields